Modeling of Artificial Muscles Made of Nylon Wire

Gabriel Madeira Fernandes da Silva
gabriel.silva@tecnico.ulisboa.pt

Instituto Superior Técnico, Lisboa, Portugal

November 2020

Abstract

Artificial muscles are an area where the bio-mechanical and bio-medical fields can merge their expertise with robotics. However, despite the effort to create new technologies or improve the existing ones, the majority of biological muscles' properties are hard to duplicate. Therefore, prosthetic devices lack optimization in weight, reliability and do not feel natural and are expensive. This is a problem for amputees in developing countries, notably children, who quickly outgrow their prostheses. Recently, a work produced supercoiled polymer actuators with fishing line, which revealed attractive properties to manufacture artificial muscles to apply in prostheses. The present work studied strategies to improve the contraction and expansion of these actuators, and built an agonist and antagonist association, with the selected solution. Grey-box modeling, based on the linear mass-spring-damper model and on the Newton's law of cooling, covered the association dynamics, together with a PID controller for the angle. Single actuators' results were in line with other works findings and revealed some degree of similarity to biological muscles' properties. Simulations and tests upon the association validated and verified the model and control scheme. It is possible to improve the results and explore new paths; still, they were satisfactory and in accordance with the expected behavior. The work also described the actuators' manufacturing process.

Keywords: artificial muscles, supercoiled polymer actuators, agonist and antagonist association, grey-box modeling, control system design

1. Introduction

Current artificial muscles solutions, like electric motors, pneumatic and hydraulic actuators cannot replicate the natural muscles' behavior yet. Possible reasons for that, as far as the author could understand, are the lack of known materials with the desired properties, or investigations aimed to the end goal - generate motion - instead of the development and test of new concepts. However, a promising method, introduced in [5], was able to produce artificial muscles made of fishing line (known as supercoiled polymer – SCP - actuators) and display attractive properties. These actuators are cheap, lightweight, flexible, silent, can work on different conditions and have a good strain level and small hysteresis, compared with other actuators [24]. Bio-mechanical and bio-medical fields can benefit from them, since reliable, lighter, more natural and cheaper prostheses are possible to obtain. This would increase the access of amputees in developing countries [1], such as children, whose prostheses quickly become impossible to wear [2].

This paper aims to provide detailed explanations about the manufacturing process of SCP actuators, but also to build and test an agonist and antagonist association (AAA) between actuators, to achieve quicker motions and showcase its applicability in prosthetic devices. This work uses grey-box modeling, based on the actuators' thermoelectric (TE) and thermomechanical (TM) properties, and a PID controller, with a filtered derivative and an anti-windup method to conduct simulations, as well. In short, the major contributions of this work are:

1. Manufacturing process systematization. Detailed description of each step, and supply of all the parameters to produce single actuators.
2. Model to describe an agonist/antagonist behavior. Implementation of an approximate AAA's model based on the works in [31, 30].
3. Tests to assess the raw material of the actuators. Assessment of the durability and elasticity to study their limiting conditions.
4. Display of a method to build an AAA. The structure works as a pair of biological muscles.

The contents of the paper are as follows: section 2 reviews artificial muscles; section 3 sets the methods adopted in the work; section 4 presents the results; and section 5 provides suggestions and conclusions.

2. Background

2.1. Biological and Artificial Muscles

Skeletal muscles are responsible for the main movements of the body; they can contract voluntarily, but can only extend passively (by gravity, contraction of an antagonist muscle or pressure of a liquid). The muscle that initiates the contraction action is the agonist and the one working in the opposite direction is the antagonist. Only the necessary agonist muscles execute the action to deliver just the proper amount of force. There are several types of contractions, but the most relevant for this work are the concentric (muscle's tension increases while its length shortens) and eccentric (tension decreases while the length increases), related to agonist and to antagonist muscles respectively [21, 16].

There are countless actuators technologies, but only a few suit artificial muscles applications. Thermally activated shape-memory alloys (SMAs) are materials that can recover the original shape when excited with a stimulus such as heat. The most popular alloy with this property is the nickel-titanium (nitinol) [15]. Pneumatic actuators entail the pressurization of a fluid in an expandable chamber to produce movement. The most common type are the braided (or McKibben) muscles [15]. Stimuli-responsive gels' working principle is due to the smart hydrogels' inner structure properties: they can swell or shrink the water with a stimulus (temperature, pH, light, electric field, chemicals, etc.) [15]. The highly oriented semi-crystalline polymer fibers comprise three types: the linear (auto and mandrel coiled actuators, i.e., SCP actuators), torsional and bending actuators. For the auto coiled actuators, the fiber twists until it coils completely onto itself, and then follows a heating process (thermal annealing) to prevent untwisting. The mandrel coiled type comprises twisting the fiber until the formation of coils, then, uses a rod to wrap the fiber around, followed by a thermal annealing process as well [7, 22, 5]. The working principle of these actuators' contraction lies on the polymer chains microscopic helical shape (acquired in the twisting process) and on the volume increase, caused by thermal heating, that induces untwisting [31]. These actuators consist of mono-filament (standard nylon) or multi-filament fibers (conductive-coated nylon). Multi-filament fibers allow the direct use of current, whereas mono-filament fibers need a resistive wire wound around them to perform the Joule heating.

2.2. Auto Coiled SCP Actuators

Manufacturing auto coiled actuators comprises two stages. The first is the twisting and coiling. The fiber should be under a certain tension with a weight hung in one end, while the other end should tie the rotating device's shaft. Low weights will tangle the fiber and heavy weights will break it. Suitable weights will form coils along the fiber, since its end does not twist. The second, is the annealing and training. The goal of the annealing is to set the polymers' structure, preventing the coils from untwisting. The literature reveals different techniques to conduct this process: there are methods via warm air (oven) [22], joule heating [7] or by plying an actuator onto itself [5]. The not plied actuators should be under a certain amount of tension too, with a fixed length, to prevent inter-coil contact [29]. The training's goal is to reach a reversible actuation response with a stimulus. Heating the coiled fiber, with a weight hung, leads to its elongation because of the high temperatures and weight. Exciting the fiber, alternating with periods of no excitation (heat/cool cycles, i.e., training cycles) will make it contract/expand between its initial resting length and a new elongated length. Performing this repeatedly will result in a length convergence point that leads to a repeatable/reversible action, whenever the process resumes [31, 30]. There are some training methods options: it can be a hydrothermal process (immersing the actuators in water) [29], via warm air (heat gun) [10] or Joule heating [31].

There are applications in the medical field that would benefit from using SCP actuators. Prosthetic-type projects developed in [1, 31, 30] were able to perform different grasping maneuvers; plus, [23, 18, 19] presented wrist and hand orthoses for rehabilitation purposes, and [3] designed a hand exoskeleton. Although these projects need improvements and lack the quality that a functional prosthesis/orthosis would require, the results showed the applicability of SCP actuators and suggested a promising path to follow in the future.

2.3. Modeling and Control

The literature reveals different methods to model and control SCP actuators. The work in [4] captured single SCP actuator's behavior based on a spring model, [23] modeled it based on a spring and damper model, to describe the input power and output force relation, and [31, 30] employed thermomechanical (based on the mass-spring-damper model) and thermoelectric models for the force and position. Moreover, there are works with nonlinear models: [9] obtained an equation to estimate the displacement; [14] proposed a model employing temperature and displacement inverse dynamics; and [13] presented nonlinear models of the temperature and of the displacement, based on the energy balance of the actuator, and on the Lagrange's equation of motion, respectively. Grey-box modeling strategies to model an antagonistic structure in [25], and in [24, 27], for a regular SCP actuator configuration, are applicable options too. Black-box strategies [8, 26], as well as the Euler-Lagrangian

approach to model the angular position of fingers' joints [19], are also methods in place. Although SCP actuators have a small hysteresis, it still occurs under certain conditions. The recurring solution to deal with this is by using inverse compensation and open-loop control with one of the following models: augmented GPI, augmented Preisach, augmented linear or the Duhem differential model [32, 33, 11].

The works in [28, 6] used control methods based on temperature measurements, via the actuator's resistance (which varies with the temperature), alongside PID controllers, to regulate the position of the actuator. Meanwhile, [4] embedded a microthermistor in the actuator to acquire the temperature, and used a proportional-differential control. The authors of [30, 31] employed open-loop control, with a lead compensator, and closed-loop control, with a feedforward design, to control the force; for the position, implemented PD and feedforward controllers. Plus, [27] proposed a control strategy based on the identified model with a feedforward controller; [25] used feedforward and PID controllers to regulate the antagonistic structure's displacement; and [14] employed a feedforward controller based on the derived nonlinear model. Other works used iterative learning control to perform trajectory tracking [17], anti-windup compensators (with a PI controller) [24], disturbance observers [26] and fuzzy control (with a PI controller too) [8].

2.4. Contraction and Expansion

The main limitation of SCP actuators is the slow heat transfer rate in the cooling process to restore the initial position, after a contraction. The literature mentions different methods to mitigate this problem. The work in [2] tested Peltier devices; [31, 30] immersed an actuator in water to identify its heating and cooling dynamics; [22, 29] explored water injection through tubes to cool the actuators; and the works [31, 30, 6] used forced air with fans. The drawbacks are the large and heavy structures (Peltier devices, fans, pumps and water reservoirs). Solutions with better designs (dissipation layers) [19], the spatial arrangement and the actuators' specs [6] can also be helpful. Moreover, it is possible to develop solutions to improve the contraction/expansion motions. [25] built an antagonistic actuator that produced force in the contraction and expansion directions, which was able to improve the expansion time; meanwhile, [17] tested a manipulator with 1 DOF with multiple antagonist SCP actuators; and [10] employed a simple symmetrical structure. The downside of these solutions is that when one actuator contracts the other resists to that motion (it expands). As a solution, the heterochiral and homochiral SCP actuators, of the association in [22], can expand and contract, simultaneously, by the action of electric current. Alternative approaches employed springs to prevent actuators to break [1], to act as an extensor element [29] and to build locking mechanisms [20]. Plus, the works [19, 1] used rubber bands to perform the extension task and to ease the overall actuation.

3. Implementation

3.1. Manufacturing Process

The paper focused on the actuators 1 and 2, but it also produced other functional actuators (with different diameters, lengths and configurations). It studied mono-filament auto coiled actuators because they fitted its purpose, and because mandrel coiled actuators were more complex to manufacture.

The method to produce SCP actuators consisted of twisting the nylon fiber until it coiled up completely, using the smallest weight that did not tangle the fiber, while preventing it from twisting together with the motor (Fig. 1 (1-2)). A reflectance sensor array counted the revolutions. The following step employed a frame to fix the resulting actuators (with a certain elongation) to avoid untwisting (Fig. 1 (3)), and an oven as well, to perform the annealing process. The temperature/time relation inside the oven avoids melting the fiber, and prevents the coils to become glued to each other. The next step was to change the fiber's attachment to the actuators' tip (Fig. 1 (4)) to obtain a more robust actuator.

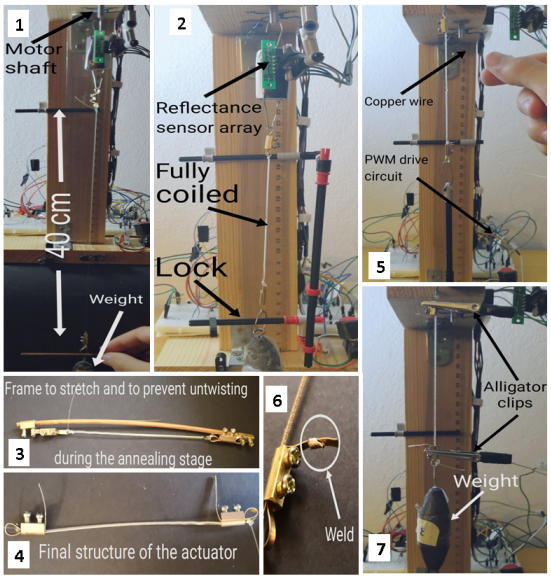

Figure 1: Steps in the twisting and coiling stage (1-2), and in the annealing and training stage (3-7).

Afterwards, the actuators' winding takes place to Joule heat and train them, using 0.10 mm diameter copper wire (Fig. 1 (5)). Note that, before welding the copper wire to each actuator's tip (Fig. 1 (6)), the distribution of its turns is key to allow a uniform heating (also note that tighter turns will break

the actuator when heated). The training, employed a weight twice as heavy as the one in the twisting and coiling stage; and the voltage values and actuation times were the combination of both that led to the fastest responses/maximum displacements, without damaging the actuators (Fig. 1 (7)). This stage used a PWM drive circuit (with a li-ion battery and an Arduino). Table 1 lists all the actuators' parameters, and Link 1 and Link 2 show their working principle and manufacturing process.

Reducing the ON time, in the first training cycle, to half is useful, since heating the actuator for the first time can break it, or lead to non-reversible elongations. The paper handled PWM values as voltage potentials (100 % duty cycle is 3.7 V).

Parameter	**Actuator 1**	**Actuator 2**
Fiber diameter	0.23 mm	0.33 mm
Fiber length	40 cm	40 cm
Load weight	40.4 g	82.7 g
Revolutions to start coiling	400	305
Total revolut.	621	500
Length	8.1 cm	8.8 cm
Frame length - elongation	9.5 cm - 117.3 %	9.9 cm - 112.5 %
Annealing specs	135 °C 12 min	
Actuator length	7.5 cm	7.5 cm
Copper length/ turns/resistance	45 cm/190 /0.96 Ω	50 cm/170 /1.07 Ω
Training specs	10x 3.26 V 5 s ON 20 s OFF w/82.7 g	10x 3.41 V 8 s ON 25 s OFF w/160.4 g
Final length - elongation	9.3 cm - 124.0 %	9.0 cm - 120.0 %

Table 1: Twisting, coiling, annealing and training parameters. The oven was preheated for 5 minutes. "Actuator length" is the length with the final structure. "Final length" is the length after training.

3.2. Contraction and Expansion

The AAA considered the inability to acquire the angle with a sensor: a card board with angle marks executed that task. The AAA has two PWM drive circuits (to handle each actuator's contraction) and a pulley. The structure is adjustable to the actuators' length to set suitable tensions. This approach tackled the slow cooling dynamics of the actuators, and improved their expansion times. The actuators were equivalent to actuator 1 since were faster (5 s) than actuator 2 (8 s) to reach the maximum displacement (and hence, angle variation). The tests were against gravity to measure angle variations associated to tensions (weights), as Fig. 2 shows. See Link 3 for a video of the AAA's working process.

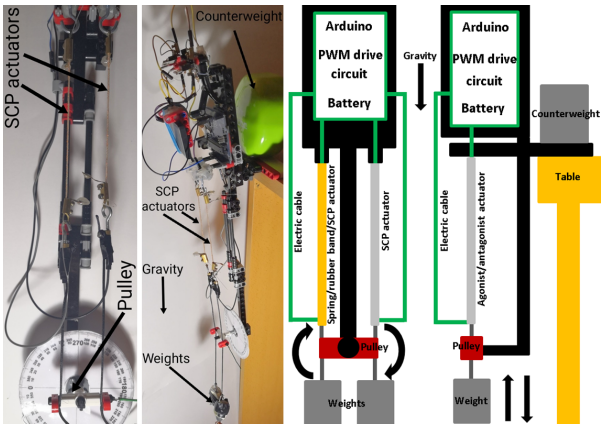

Figure 2: AAA's experimental setup and diagram. The pulley converts linear motion into an angle.

The first test was an AAA with two SCP actuators (Fig. 2). The AAA's body fixes one end of each actuator, while the other links to the pulley. The pulley rotates if one actuator contracts. The principle was to apply voltage to one actuator, inducing its contraction (agonist) and the other actuator's expansion (antagonist), simultaneously. To resume to the rest position, the roles were the inverse. Alternative tests used a spring and a rubber band as antagonists, since their contraction (after the expansion) would also expand the actuator. The tests used different weight pairs, since the stiffness values were different. The choice was to use an AAA with two actuators, because muscles can work as agonists and as antagonists, which is achievable by heating them properly. Experiments validated this choice.

3.3. Modeling Strategy

The work used grey-box modeling to model the actuator's TE and TM properties as in [31, 30]:

$$C_{th}\frac{\mathrm{d}\Delta t(t)}{\mathrm{d}t} = \frac{v^2(t)}{R} - \lambda\Delta t(t), \qquad (1)$$

$$m\frac{\mathrm{d}x^2(t)}{\mathrm{d}t^2} + \beta\frac{\mathrm{d}x(t)}{\mathrm{d}t} + kx(t) = C\Delta t(t). \qquad (2)$$

C_{th} (Ws/°C) is the thermal mass, λ (W/°C) is the absolute thermal conductivity at the ambient temperature, $v^2(t)$ (V) is the applied voltage, R (Ω) is the copper resistance, and $\Delta t(t)$ (°C) is the temperature variation from the environment to the actuator; m (kg) is the mass, k (N/m) is the spring stiffness, β (Ns/m) is the damping coefficient, C (N/°C) is a proportional coefficient, and $x(t)$ (m) is the displacement. The TE model describes the dynamics of applying voltage to the copper wire that heats the actuator. It uses the Newton's law of cooling. The TM model states how the temperature affects the displacement, and uses a linear mass-spring-damper

model. Applying the Laplace transform to (1) and (2) leads to the following transfer functions:

$$\frac{\Delta T}{V^2} = \frac{\frac{1}{RC_{th}}}{(s + \frac{\lambda}{C_{th}})}, \tag{3}$$

$$\frac{X}{\Delta T} = \frac{\frac{C}{m}}{(s^2 + s\frac{\beta}{m} + \frac{k}{m})}. \tag{4}$$

V^2 is squared to maintain the model linear. By combining (3) and (4) results in:

$$\frac{X}{V^2} = \frac{b_0}{s^3 + a_2 s^2 + a_1 s + a_0}, \quad \text{where} \tag{5}$$

$$a_2 = \frac{\beta}{m} + \frac{\lambda}{C_{th}}, \quad a_1 = \frac{k}{m} + \frac{\lambda\beta}{C_{th}m}, \quad a_0 = \frac{\lambda k}{C_{th}m} \quad \text{and} \quad b_0 = \frac{C}{C_{th}mR}. \tag{6}$$

A thermistor placed closely to the actuator acquired the temperature, and sonars acquired the actuators' displacement (Fig. 3). The sonars were not possible to mount in the AAA, which led to conduct individual displacement measurements hanging weights on each actuator. So, a specific AAA's dynamics model was not valid, unlike the adopted model for single actuators (5). Thus, the difference between the actuators' displacements will approximate the AAA's angle variation. The displacement is positive, and is the actuator's contraction.

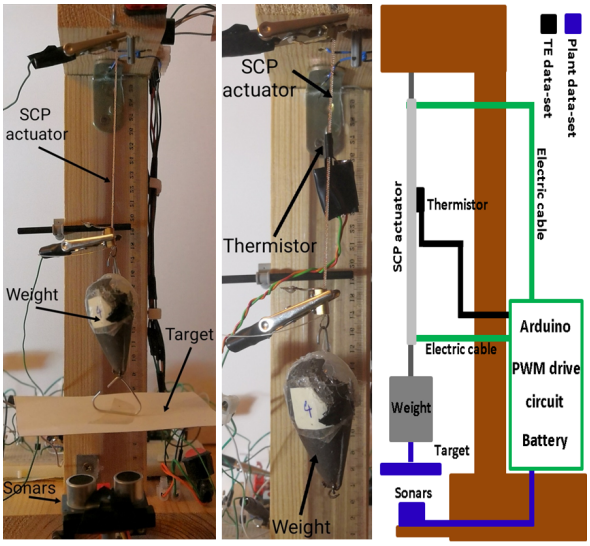

Figure 3: Setup for the plant and TE data-sets.

The data processing comprised removing the high frequency noise and off-set trends for good identification results. This stage used actuator 2, because it is less susceptible to break due to the higher diameter. The setup to acquire the data was equal to Fig. 3 – the weight was 82.7 g. The TM model data-set combined both the TE and the plant data-sets. MATLAB's system identification toolbox identified the plant's model (the coefficients were a_0=0.1909, a_1=1.2661, a_2=1.5053 and b_0=0.02995). Fig. 4 shows the data-sets, and confirms the identified model's accuracy: NRMSE ≈ 90 % and RMSE ≈ 0. These values matched other works' fitness values that used linear grey-box modeling strategies: [24] and [27] revealed NRMSEs of 90.82 % and 89.25 %, respectively, for a single actuator, and [25] obtained an NRMSE of 86.74 %, for an antagonistic structure (all for the voltage-displacement model).

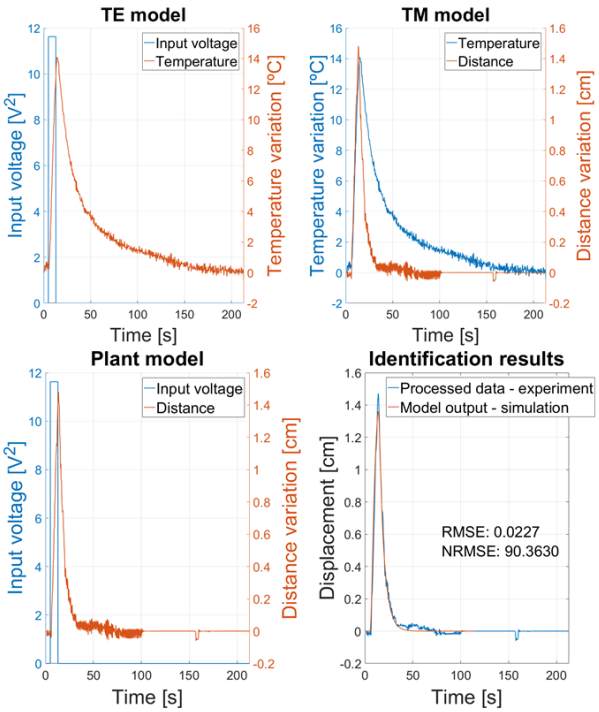

Figure 4: Processed data-sets for a voltage step difference and identification results of the plant model.

3.4. Control Strategy

With simulations it was possible to study the AAA with a feedback strategy, but the real system had to use open-loop control, inevitably. The AAA comprises two SCP actuators in parallel, so, the control scheme followed a parallel association too, since each actuator required a controller. Simulations employed a Simulink PID block with a filtered derivative (FD), to attenuate high frequency noise, and with a clamping integrator anti-windup (AW) method, to turn the integrator off properly (Fig. 5), as (7) describes. The controller's saturation limits were 0 V and 3.7[2] V, and the tests employed, once again, actuators with the same specs of actuator 2.

$$u_c(t) = K_p e(t) + K_i \int e(t) clamp(t) dt + \\ + K_d \left(\frac{de(t)}{dt} | Lowpass filter \right), \quad \text{where} \tag{7}$$

$u_c(t)$ is the PID command, K_p, K_i and K_d are the proportional, integral and derivative gains, $e(t)$ is the error and $clamp(t)$ is the condition to turn the integral off or not. The Simulink's PID tuner app tuned each PID controller's gains individually, but the process was equal for both and with the same specs. Both actuators obtained similar values, but the gains adopted opposite values, to complement their action. K_p, K_i and K_d were 0.50, 0.12 and 0.47 for the agonist, and -0.50, -0.12 and -0.47 for the antagonist; the filter coefficient was 5.84. The agonist controller/actuator in Fig. 5 can work as antagonist too - depends on the reference direction.

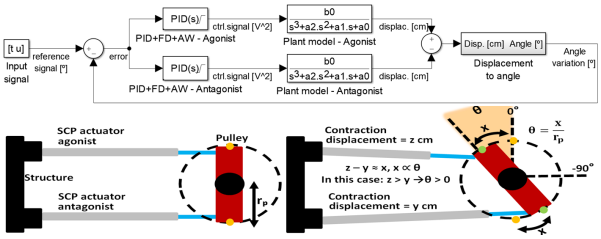

Figure 5: Block diagram of the control architecture, and geometry to estimate the AAA's angle.

4. Results

4.1. Durability and Elasticity

These experiments studied the limiting working conditions. The first assessed the temperature/time relation to set the annealing conditions. The results showed that after 12 minutes at 165 °C the actuators melted, and that at 150 °C, actuator 1 was slightly damaged and the actuator 2 was functional. The fibers' durability (standard fishing line) is low, considering the annealing temperatures/times for mono-filament actuators in the literature: [17] and [10] carried out annealing stages with 0.33 mm (at 180 °C for 15 minutes) and 0.34 mm (at >150 °C for 30 minutes) diameter fibers, respectively.

The second experiment studied the voltage (temperature) and weight relation of an actuator (Fig. 6) to set safe voltages for the training. No actuator broke, but the actuators 1 and 2 revealed non reversible elongations of 173.3 % and 133.3 %, respectively. The tests expressed that each actuator has its optimal range of operation regarding diameter, weight and voltage. Also, higher voltages induced larger elongations: actuator 1 with 3.26 V extended considerably. The temperatures read by the thermistor were lower than the real ones, and closer to the actuators' melting point (as the elongations show). This may be due to a not maximized contact surface between the sensor and the actuator.

The next experiments studied elasticity and its relation with voltage, weight and diameter of the fiber (Table 2). The first test measured the displacement, while applying successive voltage increments, with the same weight hung. The second experiment applied a fixed voltage and hung three different weights, at a time. The voltage values took into account the durability tests results, and the actuation times considered how long the actuators (with the weight hung) could handle those voltages.

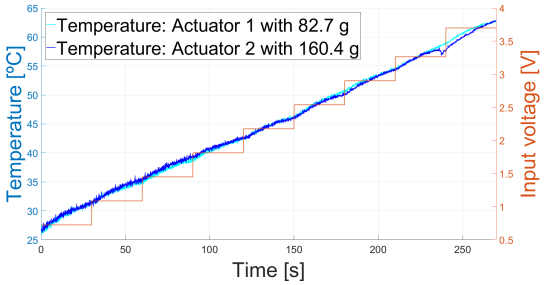

Figure 6: Temperature and weight capability.

Table 2 shows that the displacement increases gradually with higher voltages, and that there is no clear relation in the weight that leads to the maximum displacement. The values in the first experiment did not match the second experiment values for similar specs: the actuator 1 with 82.7 g reached 11.4 and 12.8 mm for 3.26 V. Besides the sonar noisy readings, this was due to different conditions: the first experiment applied successive voltages to the actuator before reaching 3.26 V. Table 3 shows that the maximum strains of actuators 1 and 2 (17.7 % and 20.4 %) agree with the literature.

PWM - Voltage	**Actuator 1** with 82.7 g	**Actuator 2** with 160.4 g
125 - 1.81 V	4.8 mm	4.1 mm
175 - 2.54 V	8.2 mm	5.6 mm
200 - 2.90 V	9.7 mm	6.6 mm
225 - 3.26 V	11.4 mm	8.7 mm
235 - 3.41 V	-	9.7 mm
Weights	with 3.26 V	with 3.41 V
40.4 g	11.8 mm	-
59.8 g	13.3 mm	-
82.7 g	12.8 mm	15.3 mm
129.4 g	-	13.3 mm
160.4 g	-	9.4 mm

Table 2: Elasticity tests results. The actuation time was 5 and 8 s for actuator 1 and 2, respectively.

4.2. Contraction and Expansion

Table 4 lists the AAA's specs. To obtain a useful and energetically efficient AAA, there is a trade-off between actuation time, resistance and supplied current. Longer actuation times (to reach the maximum displacement) will not suit prosthetic devices (despite a long-lasting battery), and short times will generally require higher electric currents, which is

Fiber	Diam. (mm)	Weight (g)	Disp. (mm)	Strain (%)
Mono.[22]	0.50	200.0	10.0	17.2
Mono.[6]	0.175	30.0	25.0	15.6
Mono.[10]	0.34	200.0	13.0	9.9
Multi.[3]	0.234	268.0	8.0	7.8
Multi.[3]	0.468	632.0	8.0	10.3

Table 3: Maximum displacements/strains of 1 ply actuators. Mono-filament fibers used copper wire.

unsafe. The energetic efficiency of the AAA's SCP actuators (Table 4) shows a fair commitment between actuation time and current that is suitable for prosthetic applications, in contrast to Table 5. The analysis ignored the need for higher voltages than 3.7 V - the focus was on the current required and on the battery's capacity (the same as the AAA).

AAA specifications & energetic efficiency	
Actuator price	≈ 0.2 €
Battery specs	3.7 Wh (3.7 V, 1000 mAh)
Mosfet specs	N channel, 30 V, 150 A
Diode specs	10 A, 1 kV
Pulley radius	15 mm
Weight	203.1 g
Dimensions	40 cm×7 cm×7 cm
Current to reach max. displacement	3.40 A / 3.19 A
Battery duration	18 min. / 19 min.
N° repetitions	216 / 142

Table 4: AAA main characteristics. The energetic efficiency values are relative to actuators 1 and 2.

Specs	[22]	[10]	[28]	[7]
Wire	copper	copper	nickel	nichrome
Res. (Ω)	2.02	1.14	1.26	19.1
Curr. (A)	5.94	1.30	0.63	0.24
Bat.(min)	10	46	95	250
Time (s)	0.625	40	65	120
N° repet.	960	69	87	125

Table 5: Energetic efficiency comparison from other works' 1 ply and mono-filament actuators. "Curr." and "Time" refer to electric current and actuation time to reach the maximum displacement.

In the experiments, the actuation time increased from 5 s (the recommended value to work at 3.26 V, for single actuators and 82.7 g) to 10 s, to cover a wider range of angle values, since no damage occurred. Table 6 shows the maximum angle variations, supplying 3.26 V for 10 s, continuously. Link 4, 5 and 6 are videos to validate the results. The data acquisition was with the naked eye, but one can say that it is better to work with two SCP actuators, since they achieve larger angle variations quicker than the spring (stiffer than actuator 1 - 165.3 N/m) and rubber band (less stiff - 38.4 N/m). The energetic efficiency is the only drawback: the spring and rubber band act passively - but it is possible to control both the agonist and antagonist actuators and resume faster to the original position.

Agonist-weight	Antag.-weight	Angle
Actr. 1 - 17.8 g	Actr. 1 - 18.3 g	20 °
Actr. 1 - 40.0 g	Actr. 1 - 40.4 g	17 °
Actr. 1 - 56.4 g	Actr. 1 - 66.3 g	15 °
Actr. 1 - 75.9 g	Actr. 1 - 82.7 g	14 °
Actr. 1 - 34.2 g	Spring - 40.4 g	9 °
Actr. 1 - 40.4 g	Spring - 59.8 g	10 °
Actr. 1 - 56.2 g	Spring - 75.9 g	8 °
Actr. 1 - 17.8 g	Rub. band - 9.0 g	12 °
Actr. 1 - 40.4 g	Rub. band - 30.5 g	12 °
Actr. 1 - 59.8 g	Rub. band - 51.2 g	11 °

Table 6: Contraction and expansion results using an AAA with 2 SCP actuators, 1 SCP actuator and 1 spring, and with 1 SCP actuator and 1 rubber band.

4.3. Model Validation and Parameters Estimation

This stage estimated the parameters of the plant's model and assessed its performance with the acquired data for a single actuator (from four input signals). Fig. 7 presents the results and proves the validity of the adopted model: the fitness level for the input step shows high confidence to follow the reference (NRMSE $\approx$ 90 %), and the remaining results also revealed good enough accuracy with more complex input signals (NRMSE values >70 %).

Appropriate equipment measured directly some model's parameters in Table 7, whereas the estimation of the remaining was via the acquired data, or with equations. Relations between power and temperature, and between energy and temperature (as in Fig. 8) from the TE model's data (during the step difference actuation) provided data to compute the absolute thermal conductivity (λ) and the thermal mass (Cth). The actuator's stiffness (k) calculation was through the slope of a linear regression between the displacements caused by the force (weight) applied on the actuator. The identification coefficients and (6) helped deriving the damping coefficient (β) and the proportional temperature to force coefficient (C): by solving b_0 in order to C, and a_2 and a_1 in order to β - which led to two solutions for β, but one was invalid.

The results for all the functional actuators were as expected: the stiffness increases with the fiber's

diameter; the thermal mass increases with the increase in the fiber's diameter and with the copper's resistance - raising the actuator's temperature requires more energy; and the damping coefficient trend is to raise its value with larger loads. From comparing the parameters with the ones in [31], one can see that k, β and C displayed a good degree of similarity, whereas C_{th}, λ and R did not. C_{th} and λ were smaller in the referred work, since it used less power to raise the actuator's temperature, probably due to a more efficient Joule heating process caused by the higher resistance of conductive fibers (i.e., a resistive wire may be inefficient to heat monofilament fibers). Different materials, manufacturing techniques (2 ply) and environmental conditions are valid reasons for the disparities too.

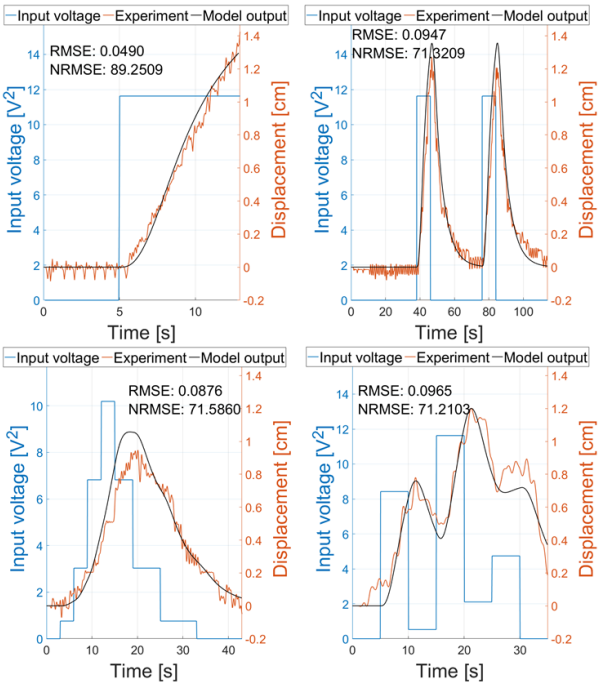

Figure 7: Model validation results and goodness of fit with independent data-sets, for actuator 2.

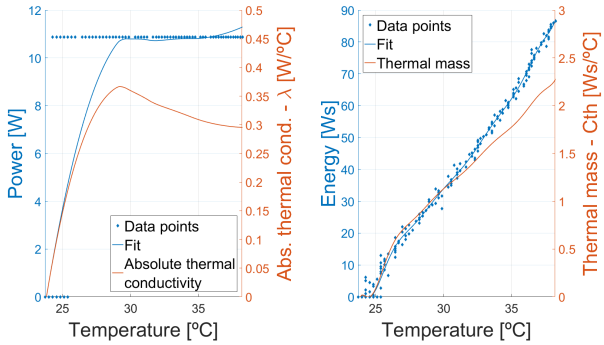

Figure 8: Absolute thermal conductivity and thermal mass computation for actuator 2.

Parameter	**Act.1**	**Act.2**	**[31]**
m (g)	44.9	87.2	100.0
R (Ω)	0.96	1.07	25.0
C (mN/°C)	1.7	6.4	2.31±0.41
β (Ns/m)	0.0303	0.1202	0.84±0.12
k (N/m)	54.49	102.84	160±35
λ (W/°C)	0.36	0.29	0.0094±0.0017
C_{th} (Ws/°C)	1.70	2.25	0.028±0.0089

Table 7: Estimated parameters of the plant's model. The mass is the actuator weight (4.5 g), plus the load weight; λ and C_{th} computation was at 31 °C and at 38 °C, for the actuator 1 and 2, respectively. The work [31] uses 2 ply and 10 cm long actuators, made of 0.38 mm diameter conductive fiber.

4.4. Simulations and Real System Performance

The next simulations studied how the AAA would behave if using a feedback control strategy.

An experiment applied a sinusoidal frequency sweep to find the highest frequency the system could track. The results showed good performance until 0.1 Hz; and that 25 ° amplitude sine waves were the highest the system could track, at that frequency. So, tests assessed the tracking performance of several references with maximum and minimum amplitudes of 25 ° and -25 °. The results revealed that the output followed, reasonably, the references and that the only downside was the lag, caused by the heating process dynamics. As a result, the RMSE values were higher than desired. Table 8 gathers data from other works, which showed better results in [17], for a smaller angle, and a closer performance in [33], for a comparable angle variation. Plus, external disturbances in Fig. 9 showed that the system can recover after ≈ 2.5 s, which is fast, considering the disturbances' magnitude and the dynamics without an antagonist. However, the voltages held the maximum value (3.7 V/13.69 V^2) briefly, which is undesirable. The control scheme had a small bandwidth (unsuited for prostheses); but, one can raise it and track faster signals: with a lead compensator, by setting different controller constraints, or with higher battery voltages.

To use open-loop control in the AAA, the acquisition of voltages fed by both PID controllers to each actuator's model, in the simulations, followed a square root computation. The result was two data-sets loaded to the Arduino (for a 0.05 Hz and 25 ° amplitude sine wave) for each actuator to use as a lookup table. The angle variation (≈ 6 °) did not follow closely the reference for ≈ 82.7 g loads (same weights of identification) hung in both actuators (see Link 7). Still, this was predictable: the model did not cover the exact AAA's dynamics, and the sine wave had the maximum trackable

amplitude (25 °) for the adopted simple model.

Control	Sine	Metric	Result
PID (AW+FD)	25° amp., 0.05 Hz	RMSE Max. error	5.77 1.34°
FF (inver. comp.) [33]	20°/45° of variation	Average error	3.4°
PI-type ILC [17]	9° amp., 0.05 Hz	Absolute error	0.6817°

Table 8: Angle tracking comparison with other works' experimental data. "Max. error" is the largest absolute error between the reference and the output, for equivalent signal sections; "ILC" means iterative learning control; "FF" means feedforward.

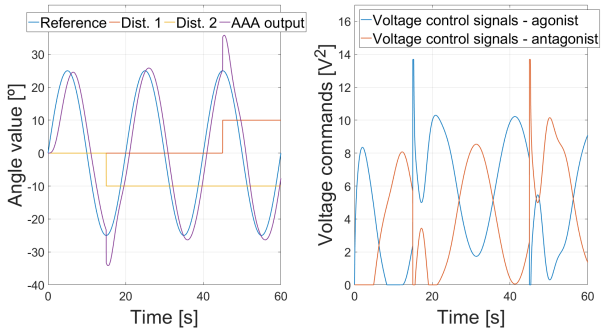

Figure 9: Simulation with external disturbances, and the required voltages to correct them.

4.5. Review Analysis

Table 9 compares an SCP actuator, the AAA and natural muscles. The AAA's parameters considered the maximum angle in Table 6, whereas the single actuator's parameters used the maximum value in Table 2, for actuator 1 with 3.26 V. Note that, the AAA's parameters used a specific TM model for the AAA (not provided in the paper) to compute each actuator's force - the main work has the full calculations. The analyses with other works in Tables 10 and 11 assess the results for their final structures (dismissing the overall quality, price and safety). The tables list eventual problems of applying those solutions in prostheses/orthoses regarding portability, performance and resemblance to muscles.

Table 9 shows that the AAA's efficiency and output work are low. In contrast, single actuators are somewhat closer to natural muscles, meaning that they have a drop of performance in the AAA. Besides this, it is possible to set relations between manufacturing parameters (Table 1) to create metrics to extrapolate the data. This is useful to produce mandrel and auto coiled actuators, knowing the fiber specs, and to automate the process. Plus, the AAA overcomes some problems of Tables 10 and 11: with angle requirements one can adapt the pulley's radius and estimate the actuators length to develop custom joint-type structures (for prostheses);

Parameter	Muscles	AAA	Actuator
Strain (%)	>40	7.3	17.7
Work dens. ($kJ.m^{-3}$)	<40	0.00255	13.1
Effic. (%)	40	0.0045	0.031
Density ($kg.m^{-3}$)	1037	103.6	3461.5
Specif. pow. ($W.kg^{-1}$)	284	0.0025	0.76
Stiff. (N/m)	Adaptab.	108.98	54.49
Stress (MPa)	0.35	3.40	4.63
Speed	Medium	Slow	Slow

Table 9: Comparison between natural muscles (values from [15, 12]), the AAA and a SCP actuator.

Drawbacks	[30]	[1]	[19]	[18]	[23]	[3]
Contraction tasks only	X	X	X	X	X	X
1 actuator to >1 joint	X	X	X	X		X
Long actrs.	X	X	X		X	
Does not use antagonist	X			X	X	X
Rub. bands		X	X			
Slow extension	X	na	na	X	X	na
Power supply	X	X	X	X	X	X
DAQ, PC			X	X	X	
CPU fans	X					
Track device			X	X	X	

Table 10: Analysis of other works' structures. The first 2 columns cover prostheses, and the remaining 4 cover orthoses. "na" means not available; "Track device" means it uses unsuitable tracking devices.

	Drawbacks
[17]	Does not link force with angle variations: actuators only contract if stretched; Setup: power supply, PC, AD/DA board.
[25]	Does not work as natural muscles: it contracts and expands; Displacement (and future angle) acquisition; Setup: power supply, PC, laser sensor, AD/DA board.
[10]	Does not work as natural muscles: the origin and insertion points have different locations; Setup: power supply.

Table 11: Antagonistic structures in other works.

it improves the expansion speed; has a small battery; and allows feedback control (only [17, 25, 23] use feedback). Long actuators may lead to large displacements (the AAA uses small actuators but has a good motion range) but have big resistances, which entails longer actuation times to contract with small voltages (unlike the AAA).

5. Conclusions

The work studied SCP actuators as an option to develop artificial muscles to match the biological muscles' main properties. It provided all the steps and parameters to manufacture functional actuators; set a safe range of work, by identifying the limiting conditions; introduced an AAA for the expansion action; and confirmed that single actuators' parameters were closer to natural muscles than the AAA's parameters (but neither one matched the muscles). Setup limitations did not allow the use of a derived AAA's model: the work adopted a simple model, based on the displacement of each actuator. Simulations showed good performance with the model, but the results in the real system were not satisfactory due to the AAA's dynamics approximation. In the future, it is important to increase the AAA's DOF, and to study techniques used in active prostheses to set a relation between user intent and movement. The path to develop artificial muscles close to skeletal muscles must be arrays of SCP actuators and its control as a whole. Searching for compliant conductive fabrics to wrap the actuators; or integrate directly SCP actuators in these fabrics' internal structure is, therefore, a must.

Single SCP actuators are easy to model, since the heat influence on the displacement describes its dynamics properly. Nevertheless, different associations between actuators (AAA) entail different dynamics, and the inclusion of hysteresis (if required) in the model may overcomplicate it. The possibility of using simple models makes the control straightforward. SCP actuators are cheap (0.2 €per unit) and easy to manufacture, even with widely available materials (the process takes time, but can be automated). Their lightweight and flexibility promote the use in artificial muscles. Also, the stress and the work density display comparable values to natural muscles. Plus, their weight lifting ability is attractive: actuator 1 lifted a weight, 18 times heavier than its weight, 17 % of its length; and actuator 2 lifted a weight, 35 times heavier, 12.5 % of its length (stiffer actuators can lift heavier weights).

The downside of SCP actuators is the low output work in contrast to the input energy, which leads to an inefficient process, probably due to a poor heat transfer rate from the copper wire to the fiber; the AAA also loses efficiency due to the antagonist opposing force. The employment in prostheses, besides an alternative and efficient heating process, requires superior batteries to increase the autonomy and to excite several actuators simultaneously. Although the low technology readiness level, some projects (of prostheses and orthoses) using SCP actuators displayed their potential; so, in a long-term period, these actuators can become a recurrent option for artificial muscles in medical devices.

References

[1] A. Arjun, L. Saharan, and Y. Tadesse. Design of a 3D printed hand prosthesis actuated by nylon 6-6 polymer based artificial muscles. In *2016 IEEE International Conference on Automation Science and Engineering (CASE)*, pages 910–915, Fort Worth TX USA, 2016.

[2] N. A. Atikah, L. Y. Weng, A. Anuar, C. C. Fat, I. Z. Abidin, and K. S. M. Sahari. Development of Nylon-Based Artificial Muscles for the Usage in Robotic Prosthetic Limb. *AIP Conference Proceedings*, 1883(1):1–8, 2017.

[3] S. Bahrami and P. Dumond. Testing of Coiled Nylon Actuators for Use in Spastic Hand Exoskeletons. In *40th Annual International Conference of the IEEE Engineering in Medicine and Biology Society (EMBC)*, pages 1853–1856, Honolulu HI USA, 2018.

[4] K. H. Cho, M.-G. Song, H. Jung, S. Y. Yang, H. Moon, J. C. Koo, J.-d. Nam, and H. R. Choi. Fabrication and modeling of temperature-controllable artificial muscle actuator. In *6th IEEE International Conference on Biomedical Robotics and Biomechatronics (BioRob)*, pages 94–98, UTown Singapore, 2016.

[5] C. S. Haines, M. D. Lima, N. Li, G. M. Spinks, J. Foroughi, J. D. W. Madden, S. H. Kim, S. Fang, M. J. de Andrade, F. Goktepe, O. Goktepe, S. M. Mirvakili, S. Naficy, X. Lepro, J. Oh, M. E. Kozlov, S. J. Kim, X. Xu, B. J. Swedlove, G. G. Wallace, and R. H. Baughman. Artificial Muscles from Fishing Line and Sewing Thread. *SCIENCE*, 343(6173):868–872, 2014.

[6] C. S. Haines and G. Niemeyer. Closed-Loop Temperature Control of Nylon Artificial Muscles. In *IEEE/RSJ International Conference on Intelligent Robots and Systems (IROS)*, pages 6980–6985, Madrid Spain, 2018.

[7] S. Horton and P. Dumond. Consistent Manufacturing Device for Coiled Polymer Actuators. In *40th Annual International Conference of the IEEE Engineering in Medicine and Biology Society (EMBC)*, pages 1849–1852, Honolulu HI USA, 2018.

[8] M. Jafarzadeh, N. Gans, and Y. Tadesse. Control of TCP muscles using Takagi–Sugeno–Kang fuzzy inference system. *Mechatronics*, 53:124–139, 2018.

[9] F. Karami and Y. Tadesse. Modeling of twisted and coiled polymer (TCP) muscle based on phenomenological approach. *Smart Materials & Structures*, 26(12):1–12, 2017.

[10] L. Li, J. Shen, J. Ma, H. Li, Y. Tian, W. Wang, X. Jia, and F. Xi. Artificial Muscles as Actuators in Symmetrical Structure. In *IEEE International Conference on Robotics and Biomimetics (ROBIO)*, pages 624–629, Kuala Lumpur Malaysia, 2018.

[11] T. A. Luong, S. Seo, J. C. Koo, H. R. Choi, and H. Moon. Differential hysteresis modeling with adaptive parameter estimation of a super-coiled polymer actuator. In *14th International Conference on Ubiquitous Robots and Ambient Intelligence (URAI)*, pages 607–612, Jeju South Korea, 2017.

[12] J. D. W. Madden, N. A. Vandesteeg, P. A. Anquetil, P. G. A. Madden, A. Takshi, R. Z. Pytel, S. R. Lafontaine, P. A. Wieringa, and I. W. Hunter. Artificial muscle technology: physical principles and naval prospects. *IEEE Journal of Oceanic Engineering*, 29(3):706–728, 2004.

[13] K. Masuya, S. Ono, K. Takagi, and K. Tahara. Nonlinear dynamics of twisted and coiled polymer actuator made of conductive nylon based on the energy balance. In *IEEE International Conference on Advanced Intelligent Mechatronics (AIM)*, pages 779–784, Munich Germany, 2017.

[14] K. Masuya, S. Ono, K. Takagi, and K. Tahara. Feedforward Control of Twisted and Coiled Polymer Actuator Based on a Macroscopic Nonlinear Model Focusing on Energy. *IEEE Robotics and Automation Letters*, 3(3):1824–1831, 2018.

[15] S. M. Mirvakili and I. W. Hunter. Artificial Muscles: Mechanisms, Applications, and Challenges. *Advanced Materials*, 30(6):1–28, 2018.

[16] J. E. Muscolino. *Cinesiologia, o sistema esquelético e a função muscular*. Lusodidacta, Loures, 1^{st} edition, 2008.

[17] S. Ono, K. Masuya, K. Takagi, and K. Tahara. Trajectory tracking of a one-DOF manipulator using multiple fishing line actuators by iterative learning control. In *IEEE International Conference on Soft Robotics (RoboSoft)*, pages 467–472, Livorno Italy, 2018.

[18] A. G. Patino, A. Ferrone, C. G. D. Gastelum, and C. Menon. A Novel Biomedical Technology Based on the Use of Artificial Muscles to Assist with Hand Functions. In *IEEE 9th Annual Information Technology, Electronics and Mobile Communication Conference (IEMCON)*, pages 620–625, Vancouver BC Canada, 2018.

[19] L. Saharan, M. J. de Andrade, W. Saleem, R. H. Baughman, and Y. Tadesse. iGrab: hand orthosis powered by twisted and coiled polymer muscles. *Smart Materials & Structures*, 26(10):1–14, 2017.

[20] L. Saharan and Y. Tadesse. Robotic hand with locking mechanism using TCP muscles for applications in prosthetic hand and humanoids. In *SPIE Smart Structures and Materials + Nondestructive Evaluation and Health Monitoring*, Las Vegas NV USA, 2016.

[21] R. R. Seeley, T. D. Stephens, and P. Tate. *Anatomia e Fisiologia, 8.ª Edição*. Lusociência, Loures, 8^{th} edition, 2011.

[22] A. N. Semochkin. A device for producing artificial muscles from nylon fishing line with a heater wire. In *IEEE International Symposium on Assembly and Manufacturing (ISAM)*, pages 26–30, Fort Worth TX USA, 2016.

[23] L. Sutton, H. Moein, A. Rafiee, J. D. W. Madden, and C. Menon. Design of an assistive wrist orthosis using conductive nylon actuators. In *6th IEEE International Conference on Biomedical Robotics and Biomechatronics (BioRob)*, pages 1074–1079, UTown Singapore, 2016.

[24] M. Suzuki and N. Kamamichi. Control of twisted and coiled polymer actuator with antiwindup compensator. *SMART MATERIALS AND STRUCTURES*, 27(7):1–9, 2018.

[25] M. Suzuki and N. Kamamichi. Displacement control of an antagonistic-type twisted and coiled polymer actuator. *SMART MATERIALS AND STRUCTURES*, 27(3):1–10, 2018.

[26] M. Suzuki and N. Kamamichi. Robust control with disturbance observer for twisted and coiled polymer actuator. *SMART MATERIALS AND STRUCTURES*, 27(8):1–9, 2018.

[27] M. Suzuki and N. Kamamichi. Simple controller design based on internal model control for twisted and coiled polymer actuator. *Actuators*, 7(3):1–13, 2018.

[28] X. Tang, K. Li, W. Chen, D. Zhou, S. Liu, J. Zhao, and Y. Liu. Temperature self-sensing

and closed-loop position control of twisted and coiled actuator. *Sensors & Actuators: A. Physical*, 285:319–328, 2019.

[29] L. Wu, M. Andrade, R. Rome, C. Haines, M. Lima, R. Baughman, and Y. Tadesse. Nylon-muscle-actuated robotic finger. In *SPIE Smart Structures and Materials + Nondestructive Evaluation and Health Monitoring*, San Diego CA USA, 2015.

[30] M. C. Yip and G. Niemeyer. High-performance robotic muscles from conductive nylon sewing thread. In *IEEE International Conference on Robotics and Automation (ICRA)*, pages 2313–2318, Seattle Washington, 2015.

[31] M. C. Yip and G. Niemeyer. On the Control and Properties of Supercoiled Polymer Artificial Muscles. *IEEE Transactions on Robotics*, 33(3):689–699, 2017.

[32] J. Zhang, K. Iyer, A. Simeonov, and M. C. Yip. Modeling and Inverse Compensation of Hysteresis in Supercoiled Polymer Artificial Muscles. *IEEE Robotics and Automation Letters*, 2(2):773–780, 2017.

[33] J. Zhang, A. Simeonov, and M. C. Yip. Three-dimensional hysteresis compensation enhances accuracy of robotic artificial muscles. *Smart Materials & Structures*, 27(3):1–17, 2018.